ChemComm

COMMUNICATION

View Article Online
View Journal | View Issue

Cite this: *Chem. Commun.*, 2026, **62**, 4094

Received 9th December 2025,
Accepted 26th January 2026

DOI: 10.1039/d5cc06993a

rsc.li/chemcomm

Consequences of encapsulated *vs.* covalently attached Pd-NHC amphiphilic polymeric nanocatalysts in bioorthogonal catalysis

Lieke de Jonge, Ibai Hazenberg, Harshit Singh, Tessa Loman, A. P. Prakasham * and Anja R. A. Palmans *

A comparison between novel Pd-NHC (N-heterocyclic carbene) catalysts covalently and non-covalently attached to polymeric nanoparticles reveals that hydrophobic domains in the vicinity of the Pd catalysts aid catalytic activity, and covalent attachment reduces cytotoxicity, opening new avenues to tune bioorthogonal reactivity of TMC-based nanocarriers.

The field of bioorthogonal chemistry and catalysis has conveniently opened up numerous novel directions in biology, such as protein conjugation, cell engineering, drug delivery, antibody–drug conjugates, and *in situ* prodrug activation, to name a few.[1–3] Typically, these non-natural reactions are performed in living systems without interfering with native biological processes, which uniquely distinguishes them as 'bioorthogonal' reactions. Transition metal catalysts (TMCs) hold tremendous potential in this field by the manifold of intriguing organic transformations they catalyse.[4,5] However, their potential in complex biological environments has been hampered by toxicity, instability and deactivation, and poor solubility in aqueous media.[6] As a result, nanocarriers have been engineered to incorporate TMCs and thereby enhance their stability and improve their biocompatibility in biological media.[7,8] Of particular interest are amphiphilic heterograft polymers that collapse in water to form nanometer-sized nanoparticles (NPs) with hydrophobic interiors.[9,10] These NPs carry the TMCs within their hydrophobic core, improving water compatibility and limiting exposure of TMCs to complex media.

Recently, several advanced nanocarriers have been developed for the Pd(0/II)-mediated bioorthogonal prodye and prodrug activation in complex environments (Table S12).[11–14] We have previously developed amphiphilic heterograft polymers with PPh_3 and bipyridine pendants that complex Pd(II) and found that the resulting NPs were capable of activating prodyes and prodrugs in water as well as in complex media.[15] However, the polymers with pendant PPh_3 were highly sensitive to oxidation to the corresponding oxide, requiring demanding formulation conditions to obtain the Pd(II)-based NPs. Both the nature of the ligand and the polymer's microstructure proved important for the catalyst's activity and stability, but activity was reduced in cell culture growth media. As part of our interest in using polymeric nanoparticles as carriers for bioorthogonal catalysis,[16–18] we here focus on NHC ligands for the preparation of Pd(II) catalysts for bond cleavage activation of prodyes. Pd-NHC catalysts are highly effective in various C–X (X = C, N, O, S) bond forming reactions,[19] and also function in water.[20] Wegner *et al.* showed that incorporation of a Pd-NHC complex in the membrane of *E. coli* allowed the bioorthogonal cleavage of propargyl ethers.[21] Their simple synthesis, stability, divergent structural motifs and high metal affinity make NHC a ligand of choice in organometallic chemistry. NHC-ligands were recently used by us in combination with Cu(I), showing excellent CuAAC activity in presence of 15 mM glutathione.[22] Moreover, Cu(I)-NHC embedded in a polymer showed bioorthogonal activity in cellular media and mouse models.[23] Here, we apply NHC ligands for complexing to Pd(II) and evaluate the activity in aqueous and complex media, and compatibility with mammalian cells to assess their suitability for bioorthogonal catalysis. Particularly, we unveil the intriguing differences between physically encapsulated and covalently attached Pd-NHC to polymeric NPs, highlighting the effect of the hydrophobic micro-environment on catalyst activity, toxicity and stability.

We designed our NHC ligand with the following features: (i) presence of a fused bicyclic motif for strong coordination and steric shielding for Pd (ii) azide moiety for covalent ('click') attachment to amphiphilic polymer and (iii) $-CF_3$ label for easy NMR characterization within the polymer matrix. The $-N_3$ and $-CF_3$ group appended bicyclic 1,2,4-triazole based NHC ligand precursor (**1**) was synthesized from L-pyroglutamic acid through a sequence of manipulations (see SI for details, Scheme S1, Fig. S1-S4).[24] Pd-NHC complex (**2**) was synthesized by reacting (**1**) with $PdBr_2$ in presence of KBr, K_2CO_3 as base and pyridine

Department of Chemical Engineering & Chemistry and Institute for Complex Molecular Systems, Eindhoven University of Technology, P.O. Box 513, 5600 MB, Eindhoven, The Netherlands. E-mail: a.p.prakasham@tue.nl, a.palmans@tue.nl

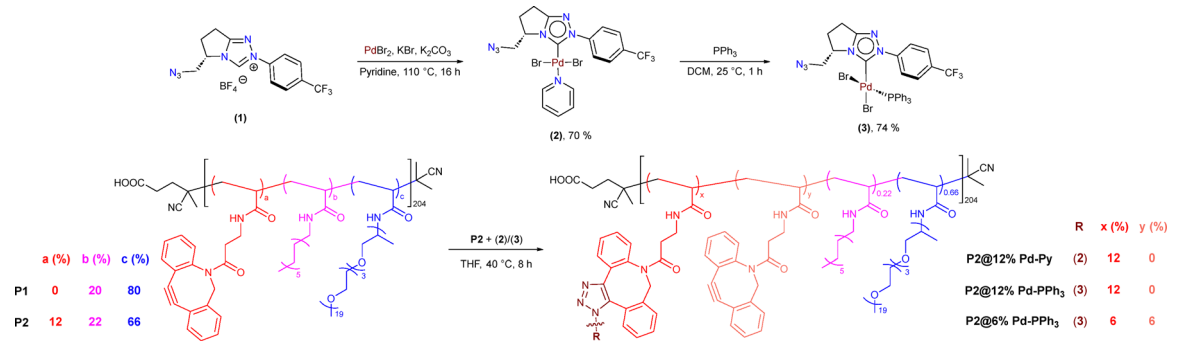

Scheme 1 Synthesis of Pd(II)-NHC complexes (**2**), (**3**) and covalently Pd-NHC functionalized amphiphilic (**P2**) polymers.

as solvent for the reaction (Scheme 1). The pyridine in complex **2** is a labile, throw away ligand, which aids the incoming substrates during the catalysis process.[25] The formation of complex (**2**) was confirmed by the disappearance of the characteristic NC*H*N resonance of the precarbene in the ^{1}H NMR while the ^{19}F{^{1}H} signal was observed at −62.51 ppm for the –C*F*$_3$ group (Fig. S5–S11).

In order to reinforce the Pd center further by the combined effect of both the phosphine and NHC ligands, complex (**3**) was made by replacing the Py ligand with a PPh_3 ligand in complex (**2**) (Fig. S12–S19). The typical Pd coordinated *cis*-*P*Ph$_3$ signal was observed at 26.20 ppm in the ^{31}P{^{1}H} NMR (Fig. S17, Table S14). The presence of –N_3 in Pd complexes (**2**) and (**3**) was confirmed using IR spectroscopy where the azido stretch appeared around 2113 cm^{-1} (Fig. S10 and S18).[26]

We incorporated the Pd complexes (**2**) and (**3**) into the amphiphilic nanoparticles by physical encapsulation as well as attached them to the heterograft polymers *via* a click reaction. For encapsulation, **P1** polymer was used, which contained 20% *n*-dodecyl chains for hydrophobic collapse and 80% Jeffamine®M1000 for water solubility. For the covalent linking, we prepared polymer **P2** with strained alkyne containing dibenzocyclooctyne (DBCO) grafts (12%) and dodecyl (22%) and Jeffamine (66%) as hydrophobic and hydrophilic grafts, respectively. Polymers **P1,2** were made by post functionalization modification of the poly(pentafluoro-phenylacrylate) using previously optimized procedures and fully characterized (Fig. S20–S31).[15] Using a strain promoted azide–alkyne cycloaddition (SPAAC) the azide functional Pd complexes were readily attached to the DBCO linked polymer backbone. Complete functionalization (12%) of **P2** was done with Pd complexes (**2**) and (**3**) to obtain polymers **P2@12% Pd-Py** and **P2@12% Pd-PPh$_3$**. In order to check the effect of catalyst concentration and polymer microstructure, half of the DBCO groups were functionalized, *i.e.*, 6%, with (**3**) affording polymer **P2@6% Pd-PPh$_3$** (Scheme 1). Here, we also aimed to study the synergistic effect of NHC and PPh_3 ligands on Pd, which is expected to enhance stability and activity in catalysis.[27–29] After post functionalization, all polymers were purified using dialysis to remove unbound grafts/Pd/free pentafluorophenol and fully characterized (Fig. S32-S40).

The presence of polymer bound Pd was confirmed by NMR where, for instance, the –C*F*$_3$ group signal was observed at −62.48 ppm and the Pd bound *P*Ph$_3$ signal was observed at 26.69 ppm for **P2@12% Pd-PPh$_3$** in their respective ^{19}F{^{1}H} and ^{31}P{^{1}H} NMR (Fig. 1A). The Pd concentration in the polymer samples was quantified using inductively coupled plasma optical emission spectroscopy (ICP-OES). The measured Pd concentrations were in good agreement with the calculated Pd concentration. The higher concentration measured for **P2@12% Pd-PPh$_3$** suggests that the excess Pd complex used in the click reaction was not completely removed by dialysis (Fig. 1B). After formulating the obtained **P1,2**-based polymers into NPs in water, dynamic light scattering (DLS) showed hydrodynamic radii (R_H) of the NPs around 6.5–11.6 nm, similar to the ones previously reported (Table S1 and Fig. S41).[15]

More detailed insights into the nature of the NPs were obtained from small angle X-ray scattering (SAXS) analysis in water (SI Section 4.4). The experimental SAXS curves (Fig. 1C)

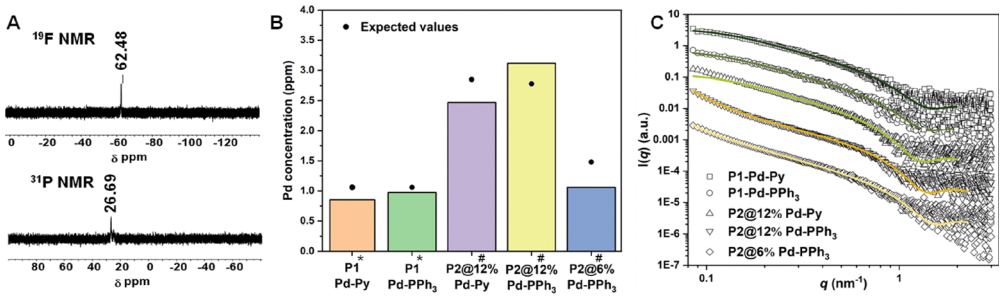

Fig. 1 (A) ^{19}F{^{1}H} and ^{31}P{^{1}H} NMR of **P2@12% Pd-PPh$_3$**; (B) Pd quantification by ICP-OES measured in milliQ water (*) or 2% THF in milliQ water (#); (C) experimental SAXS curves (symbols) and worm-like chain form factor fits (lines) for Pd-based NPs.

show global shapes indicative of conformationally stretched chains with limited flexibility for all NPs, similar to our previously studied copolymers lacking Pd complexes.[30] The experimental data were fit to the previously applied semiflexible worm-like chain model.[29] Comparison of the two encapsulated **P1** NPs revealed that the form factor fits (details in SI, Table S4) were in good agreement with the experimental data. The Kuhn length l_k, *i.e.* the distance over which the polymer is rigid, was around 9 nm for **P1**-based NPs containing encapsulated Pd catalysts, similar to the previously studied Jeffamine-based NPs with only hydrophobic grafts.[30]

The shape of the scattering curve obtained for **P2@12% Pd-Py** closely resembled that of **P1-Pd-Py**, indicating that nanoparticle shape and compactness are not significantly affected by physical encapsulation or covalent attachment. **P2**-based NPs showed some aggregation as evidenced by the upturn at low q values. This effect was more pronounced for the 12% functionalized particles and the PPh_3 comprising polymers. To account for the aggregation, we adapted our fitting strategy by combining a power-law model with the flexible cylinder model to extract data from the scattering curves for **P2**-based polymers (Fig. 1C). This afforded good fits. Notably, the Kuhn lengths l_k of **P2**-based polymers were comparable to the **P1**-based polymers, albeit that l_k was slightly higher ($\approx$16.0 nm) for **P2@12% Pd-PPh$_3$**, suggesting a lower flexibility (Table S4).

The hydrophobic interior of the NPs not only comprise the hydrophobic catalysts, but also sequester hydrophobic substrates in water.[31] We applied two different prodyes, pro-2,4-dinitro phenol (**4**) and pro-coumarin (**6**) to test the TMC activation strategy as this allows real time monitoring of the catalytic process by absorption or fluorescence spectroscopy, respectively. To start with, we studied the depropargylation reaction of *O*-propargylated 2,4-dinitro phenol (**4**) using the new Pd-NHC NPs (Scheme 2). The reactions were performed in water (37 °C) using a substrate to catalyst S/C ratio of 10/3 (100 μM substrate, 30 μM Pd). The formation of the dye, 2,4-dinitro phenol (**5**) was monitored using UV-Vis spectroscopy at λ = 400 nm. The encapsulated **P1** particles steadily cleaved the *O*-propargyl group of the pro-DNP in water over 12 h. **P1-Pd-Py** NPs showed slightly better activity than the **P1-Pd-PPh$_3$** NPs (Fig. 2A). Also the **P2**-based NPs showed good activity in water and both the covalently attached **P2@12% Pd-Py** and **P2@12% Pd-PPh$_3$** NPs showed similar behavior. Interestingly, increasing the polymer concentration while keeping the S/C ratio constant by comparing **P2@12% Pd-PPh$_3$** to **P2@6% Pd-PPh$_3$** (Fig. 2B) revealed notable differences, with the latter system showing a higher activity. This indicated that the presence of more hydrophobic compartments in **P2@6% Pd-PPh$_3$** benefits the rate of the deprotection reaction while keeping the overall Pd concentration constant. This is also obvious from the Pd to polymer (P) ratio, where Pd : P is 24 : 1 for **P2@12% Pd-PPh$_3$** while it is 12 : 1 for **P2@6% Pd-PPh$_3$** with an overall [Pd] of 30 μM in both cases (Table S5). The enhanced activity observed for the **P2@6% Pd-PPh$_3$** NPs suggests that more hydrophobic domains are more beneficial than a higher local concentration of Pd. Additionally, the higher Kuhn length observed for **P2@12% Pd-PPh$_3$** suggested a less dynamic polymer chain adopting more compact conformations. Such rigidity can restrict segmental motion and diffusion pathways, partially shielding catalytic sites and reducing substrate accessibility, eventually leading to diminished catalytic activity. All the experiments were repeated at least four times to ensure reproducibility and consistency of the observed trend.

The average catalytic activity of different polymeric NPs was compared against $T_{1/2}$, the time it takes to reach 50% formation of DNP (**5**), approximated by an absorbance of 0.3 at 400 nm in the UV-Vis spectrum (see SI section 5.1 for details). Fig. 2B showed that encapsulated **P1-Pd-Py** is the fastest and covalent **P2@6% Pd-PPh$_3$** is faster than **P2@12% Pd-PPh$_3$** when keeping the S/C ratio constant. Additionally, the formation of DNP (**5**) was quantified by HPLC after 24 h (SI section 5.2; Table S7). Analyzing all reactions after 24 h with a S/C ratio of 10/3 showed higher amounts of DNP formed for the covalent systems compared to the encapsulated systems (Fig. 2C). In fact, after 24 h, the best performing covalent system, **P2@6% Pd-PPh$_3$** showed full conversion, whereas the best performing encapsulated **P1-Pd-Py** had a conversion of 87% to DNP. In addition, **P1-Pd-PPh$_3$** showed a 58% formation of DNP. The results show that the covalent systems outperformed the encapsulated system. This aligns with our previous observations where a $PdPPh_3$ complex encapsulated into NPs was slower than covalently crosslinked $PdPPh_3$ complexes.[15] However, the observed activity of these novel NHC-Pd-based NPs was lower (full conversion after 24 h) than our previous NPs (full conversion after 3.3 h, for same S/C 10/3), confirming the important role of the ligand and polymer microstructure for better catalytic activity.[32] The differences between **P1** and **P2** extend beyond the mode of catalyst attachment and also include variations in Pd : P ratio, polymer graft composition and hydrophobic domain content, all of which may contribute to the observed differences in catalytic activity.

To assess the cytotoxicity of the novel catalytic systems, important for bioorthogonal reactivity, all Pd NPs were incubated with HeLa cells for 24 h. The cell viability was tested using the CCK-8 assay. The results showed that the encapsulated **P1** NPs exhibited more pronounced toxicity than the covalently attached **P2** NPs. **P2@12% Pd-PPh$_3$** NPs was the least toxic after 24 h of incubation (Fig. S61). Even at high Pd concentrations of 100 μM, the cell viability remained high. This finding emphasizes the beneficial effect of having covalently attached Pd catalysts in the polymer chain for better biocompatibility.

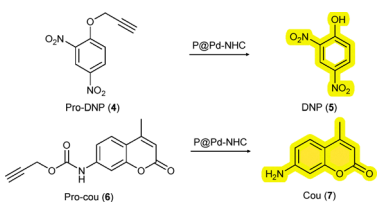

Scheme 2 Model prodye activation using Pd nanoparticles.

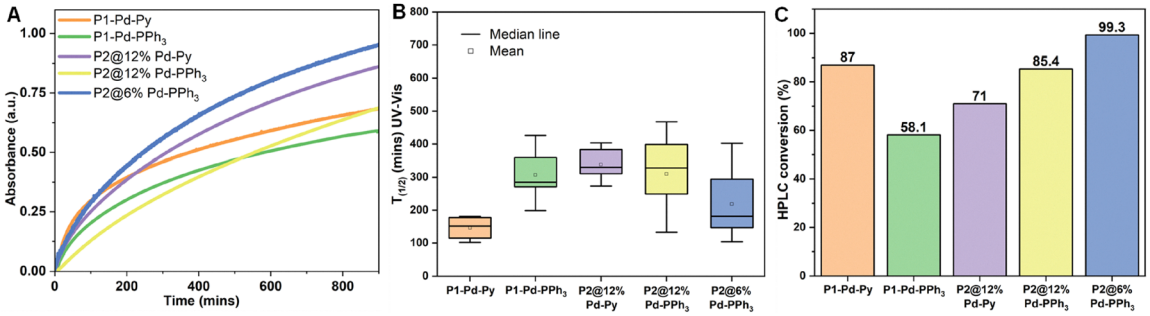

Fig. 2 (A) Kinetic profiles of encapsulated **P1** and covalently attached **P2** NPs in a pro-DNP (**4**) (100 μM) to DNP (**5**) conversion monitored by UV-Vis over time at λ = 400 nm in water at 37 °C using 30 μM of Pd; (B) $T_{1/2}$ comparison of the **P1** and **P2** NPs in the formation of DNP (**5**); $T_{1/2}$ (time taken for 50% formation of DNP (**5**) by UV-Vis, mean of multiple runs); (C) HPLC conversion of DNP (**5**) after 24 h.

Having established that some of the novel catalytic NPs show good compatibility with mammalian cells, we finally tested the reactivity of the new catalysts in complex media. To this end, all reactions were repeated in PBS and the cell culture media, RPMI (preferred growth media for suspension cell lines) and DMEM (preferred for adherent cell lines). Cell culture media are a good predictor for catalyst activity in *in vitro* conditions.[33] The catalytic activity was mostly retained in PBS with **Pd-Py** containing NPs showing enhanced activity. Unfortunately, activity was mostly lost in RPMI and DMEM (Fig. S47), also for the most active **P2@6% Pd-PPh$_3$**. Changing the substrate from pro-DNP to pro-cou (**6**) (SI Section 5.3) containing a carbamate protecting group showed a similar trend in water, whereas in presence of cell culture media did not result in the formation of fluorescent dye (**7**). The loss of Pd activity in cell culture media prompted the investigation of deactivation pathways. Substrate activation studies in presence of 30 μM of various biomolecules revealed strong inhibition by L-histidine, L-cysteine and glutathione for both **P1** and **P2** NPs, consistent with Pd catalyst poisoning by amine and sulfur nucleophiles (Fig. S48). This is in line with the results of Wegner *et al.* where the catalytic reactions worked when performed in buffered conditions with *E. coli*, but failed for mammalian cells.[21] Lastly, the reusability of the Pd NPs was evaluated by re-adding the substrate after the first run (15 h), and the Pd NPs remained active even after 30 h continuously cleaving the substrate in water (Fig. S49).

In summary, we developed novel Pd-NHC based polymeric nanoparticles and investigated their potential for bioorthogonal bond cleavage reactions. Covalently Pd-NHC attached NPs performed better than the encapsulated ones and the **P2@6% Pd-PPh$_3$** NPs with more hydrophobic micro-environment performed the best for prodye activation reactions in water. Additionally, the covalently linked **P2** NPs were less toxic to HeLa cells than the physically encapsulated **P1** NPs. Despite improved aqueous activity and reduced toxicity, Pd nanoparticles remained susceptible to deactivation by biological nucleophiles. Strategies such as the incorporation of chelate stabilizing ligands, polymer compartmentalization and cross-linking to enhance catalyst protection are underway in our laboratory.

Conflicts of interest

There are no conflicts to declare.

Data availability

Supplementary information: experimental procedures, characterization and spectroscopic data; ^{1}H, ^{13}C{^{1}H}, ^{19}F{^{1}H}, ^{31}P{^{1}H} NMR, MALDI-ToF-MS spectra of Pd-NHCs, GPC, DLS, ICP-OES, SAXS data of polymers, UV-Vis and fluorescence data, HPLC data of the kinetics runs are available in the electronic supplementary information (SI). See DOI: https://doi.org/10.1039/d5cc06993a. The SAXS data related to this article is available in DOI: https://doi.org/10.15151/ESRF-ES-2010314049.

Acknowledgements

The project has received funding from the European Union's Horizon 2020 research and innovation program under the Marie Skłodowska-Curie grant agreement no. 899987. We gratefully acknowledge support by The Dutch Research Council (NWO Gravitation; IPM program), the TU/e and Peter Lipman for ICP-OES analysis. We thank the staff of the ESRF and EMBL Grenoble for assistance and support in using beamline BM29 under proposal number MX-2677.

References

1 F. M. Zielke and F. P. J. T. Rutjes, *Top. Curr. Chem.*, 2023, **381**, 35.
2 W. Wang, X. Zhang, R. Huang, C.-M. Hirschbiegel, H. Wang, Y. Ding and V. M. Rotello, *Adv. Drug Delivery Rev.*, 2021, **176**, 113893.
3 E. M. Sletten and C. R. Bertozzi, *Angew. Chem., Int. Ed.*, 2009, **48**, 6974–6998.
4 J. H. Docherty, T. M. Lister, G. Mcarthur, M. T. Findlay, P. Domingo-Legarda, J. Kenyon, S. Choudhary and I. Larrosa, *Chem. Rev.*, 2023, **123**, 7692–7760.
5 U. Bin Kim, D. J. Jung, H. J. Jeon, K. Rathwell and S. Lee, *Chem. Rev.*, 2020, **120**, 13382–13433.
6 J. Miguel-Ávila, M. Tomás-Gamasa and J. L. Mascareñas, *Trends Chem.*, 2023, **5**, 474–485.
7 A. A. H. Laporte and J. N. H. Reek, *Chem. Rev.*, 2025, **125**, 7223–7274.
8 F. Huang, J. Liu, M. Li and Y. Liu, *J. Am. Chem. Soc.*, 2023, **145**, 26983–26992.
9 A.-S. Glaive, C. Le Cœur, J.-M. Guigner, C. Amiel and G. Volet, *Langmuir*, 2024, **40**, 2050–2063.

10 J. Odrobińska, M. Skonieczna and D. Neugebauer, *Int. J. Mol. Sci.*, 2021, **22**, 1202.
11 R. Martínez, C. Carrillo-Carrión, P. Destito, A. Alvarez, M. Tomás-Gamasa, B. Pelaz, F. Lopez, J. L. Mascareñas and P. del Pino, *Cell Rep. Phys. Sci*, 2020, **1**, 100076.
12 E. Indrigo, J. Clavadetscher, S. V. Chankeshwara, A. Megia-Fernandez, A. Lilienkampf and M. Bradley, *Chem. Commun.*, 2017, **53**, 6712–6715.
13 J. Li, J. Yu, J. Zhao, J. Wang, S. Zheng, S. Lin, L. Chen, M. Yang, S. Jia, X. Zhang and P. R. Chen, *Nat. Chem.*, 2014, **6**, 352–361.
14 B. J. Stenton, B. L. Oliveira, M. J. Matos, L. Sinatra and G. J. L. Bernardes, *Chem. Sci.*, 2018, **9**, 4185–4189.
15 A. Sathyan, S. Croke, A. M. Pérez-López, B. F. M. de Waal, A. Unciti-Broceta and A. R. A. Palmans, *Mol. Syst. Des. Eng.*, 2022, **7**, 1736–1748.
16 A. Sathyan, E. Archontakis, A. J. H. Spiering, L. Albertazzi and A. R. A. Palmans, *Molecules*, 2024, **29**, 1850.
17 L. Deng, A. Sathyan, C. Adam, A. Unciti-Broceta, V. Sebastian and A. R. A. Palmans, *Nano Lett.*, 2024, **24**, 2242–2249.
18 A. Sathyan, T. Loman, L. Deng and A. R. A. Palmans, *Nanoscale*, 2023, **15**, 12710–12717.
19 N. Muniyappan and S. Budagumpi, *Inorg. Chim. Acta*, 2026, **589**, 122915.
20 E. Levin, E. Ivry, C. E. Diesendruck and N. G. Lemcoff, *Chem. Rev.*, 2015, **115**, 4607–4692.
21 T. Wegner, A. Dombovski, K. Gesing, A. Köhrer, M. Elinkmann, U. Karst, F. Glorius and J. Jose, *Chem. Sci.*, 2023, **14**, 11896–11906.
22 A. P. Prakasham, H. Singh and A. R. A. Palmans, *Chem. Commun.*, 2025, **61**, 9697–9700.
23 D. Zheng, J. Tao, L. Jiang, X. Zhang, H. He, X. Shen, Y. Sang, Y. Liu, Z. Yang and Z. Nie, *J. Am. Chem. Soc.*, 2025, **147**, 998–1007.
24 J. Brand, J. Siles and J. Waser, *Synlett*, 2010, 881–884.
25 M. Kumar Gangwar, S. Dey, A. P. Prakasham. and P. Ghosh, *Polyhedron*, 2021, **197**, 115011.
26 J. Y. Park, H.-J. Kwon, S. Mondal, H. Han, K. Kwak and M. Cho, *Phys. Chem. Chem. Phys.*, 2020, **22**, 19223–19229.
27 E. Bortolamiol, G. Isetta, I. Caligiuri, N. Demitri, S. Paganelli, F. Rizzolio, T. Scattolin and F. Visentin, *Eur. J. Inorg. Chem.*, 2023, e202300084.
28 A. Kumar, M. K. Gangwar, A. P. Prakasham, D. Mhatre, A. Ch Kalita and P. Ghosh, *Inorg. Chem.*, 2016, **55**, 2882–2893.
29 T. E. Schmid, D. C. Jones, O. Songis, O. Diebolt, M. R. L. Furst, A. M. Z. Slawin and C. S. J. Cazin, *Dalton Trans.*, 2013, **42**, 7345.
30 S. Wijker, D. Dellemme, L. Deng, B. Fehér, I. K. Voets, M. Surin and A. R. A. Palmans, *ACS Macro Lett.*, 2025, **14**, 428–433.
31 M. Artar, E. R. J. Souren, T. Terashima, E. W. Meijer and A. R. A. Palmans, *ACS Macro Lett.*, 2015, **4**, 1099–1103.
32 J. Willenbacher, O. Altintas, V. Trouillet, N. Knöfel, M. J. Monteiro, P. W. Roesky and C. Barner-Kowollik, *Polym. Chem.*, 2015, **6**, 4358–4365.
33 Y. Liu, S. Pujals, P. J. M. Stals, T. Paulöhrl, S. I. Presolski, E. W. Meijer, L. Albertazzi and A. R. A. Palmans, *J. Am. Chem. Soc.*, 2018, **140**, 3423–3433.

